Journal of Thermal Analysis and Calorimetry, Vol. 73 (2003) 361–380

EFFECT OF THE IONIC AGGREGATION ON THE CRYSTALLIZATION BEHAVIOR OF POLY(ETHYLENE) PART OF IONOMER

Y. Gao[1], *N. R. Choudhury*[1*], *N. Dutta*[1], *R. Shanks*[2] *and R. Weiss*[3]

[1]Ian Wark Research Institute, University of South Australia, Mawson Lakes, South Australia, Australia
[2]Royal Melbourne Institute of Technology, LaTrobe Street, Melbourne,Victoria, Australia
[3]Institute of Materials Science, University of Connecticut, Storrs, CT, USA

(Received May 6, 2002; in revised form January 2, 2003)

Abstract

The influence of ionic interaction on the melt-crystallization behavior of the ethylene ionomer was studied using modulated DSC (MDSC^{TM}), wide angle X-ray scattering (XRD) and hot stage microscopy. The kinetics of the crystallization process of the ionomer was evaluated using isothermal differential scanning calorimetry (iso-DSC). Wide-angle X-ray scattering was used to examine the *d* spacing of poly(ethylene) part. The crystallinity of the poly(ethylene) part of ionomer measured from XRD is found to be 24%, which is comparable to that obtained from MDSC^{TM}. Small-angle X-ray scattering (SAXS) results show that the clusters and multiplets exist in the ionomer, and the cluster is about 127 Å. The kinetics of crystallization process obtained using Avrami equation shows that the crystallization process is fundamentally similar to poly(ethylene) as it goes through nucleation and propagation stages of the crystals. However, the morphology of the crystal appears to be different and influenced by clusters (platelike and/or needle-shaped) as evident from Avrami constant. This is different from the poly(ethylene) (which is spherulitic in nature) due to polar cluster and hydrophobic PE melt interaction.

Keywords: ionic aggregation**,** iso-DSC, kinetics of crystallization, MDSC, melt-crystallization, poly(ethylene)

Introduction

Ethylene ionomers are thermoplastic polymers containing polyolefin backbones and a relatively small number, i.e., <15 mol% of ionic groups, such as carboxylic, sulfonic, and phosphoric acids, etc. [1, 2]. Most commonly, the acid groups are partially or fully neutralized to form salt group substituents, either showing as pendant groups or directly incorporated into the main chain. The presence of only a small number of ionic groups strongly affects the properties of the polymer by creating

* Author for correspondence: E-mail: namita.choudhury@unisa.edu.au

1388–6150/2003/ $ 20.00
Akadémiai Kiadó, Budapest

strong intramolecular and intermolecular secondary bonding forces. Thus ethylene ionomers possess three distinct phases: crystalline, amorphous phases and ionic aggregates. The aggregates act as labile physical crosslink and influence the stability and reversibility of the crystalline phase over time.

Extensive reports on the microstructure and properties of ionomers have been published so far. The ionic cluster models have been proposed, and evidenced by various techniques, such as small-angle X-ray scattering (SAXS), dynamic mechanical analysis, dielectric measurements, electron microscopy, and electron spin resonance spectroscopy [3–21]. It is also well known that the acid and salt groups are resident in the amorphous phase and at the amorphous-crystal interface [15]. However, it is important to understand whether the ease of crystal formation and its morphology are affected due to copolymerization of poly(ethylene) (PE) with acrylic acid followed by ionization. The most important parameter that influences the cluster formation is the strength of ionic interaction between the ion pairs. This is again dependent on the valency and size of the ions. Small and highly polar ions can interact stronger than the larger ions. Despite the amount of research performed on the PE crystal structure, the effect of ionic aggregation on the crystallinity and the stability/reversibility of such crystal structure over time have not been fully understood.

In general, the properties of a semicrystalline material depend on the morphology developed during processing. Again, the morphology is controlled by kinetics and mechanism of crystallization. Differential scanning calorimetry (DSC) is a widely used thermal technique to get quantitative information about melting and crystallinity that involves endothermic or exothermic processes, or changes in heat capacity. Isothermal DSC (iso-DSC) is an excellent tool to evaluate the kinetics of the crystallization process. The DSC data can be analyzed to determine the number of nuclei and mode of crystallization using the Avrami equation [22], and the kinetic parameters of crystallization using the Arrhenius equation and the Sestak-Berggren equation (SB) [23]. So far, the studies on the kinetics of polymer crystallization process have been done [24–26] with several nucleators such as metal carboxylates for polyolefins. Hirasawa *et al*. [27] studied the effect of metal cation type on the ionomer structure and the properties of the ionomer using thermal analysis and mechanical testing. They noted the change in DSC thermal data with neutralization by type of cation. As the ionomer undergoes transitions, which are very complex (multiple thermal processes), it is often difficult to interpret the heat flow from the DSC experiment properly. The unique ability of Modulated Differential Scanning Calorimetry (MDSC™) is to monitor such complex compounds/processes and to identify weak transitions. MDSC™ [28–30] is the extension of DSC. MDSC^{TM} provides not only the same information as conventional DSC, but also provides unique information not available from conventional DSC. MDSC^{TM} allows the total heat flow to be separated into the reversing and the non-reversing parts and gives insight to the complex transitions. While crystallization behavior of PE is well documented, there are very few reports on the crystallization of ethylene ionomers [31–34]. In this work, we have investigated the effect of the ionic aggregation on the melt-crystallization behavior of poly(ethylene) ionomer. Iso-DSC and MDSC^{TM} were used to gain under-

standing of the crystalline structure of the ionomer and to enhance the quality and the amount of information of its melt-crystallization behaviour. Iso-DSC was used to study the kinetics of melt-crystallization behavior of polyethylene part of ionomer. MDSC^{TM} was primarily used to evaluate the nature of ionic cluster melting. The morphology of Zn-PEAA was established by small-angle X-ray scattering (SAXS). Wide-angle X-ray diffraction study was carried out to evaluate the crystallinity and *d* spacing of this sample.

Experimental

Materials

Iotek 4200-poly(ethylene) acrylic acid neutralized by zinc salt (Zn-PEAA) is received from Kemcor Australia, which was produced by EXXON. Acrylic acid content in the copolymer was 11 mass%, and 14 mol% of total carboxyl groups was neutralised by zinc salt. The chemical structure of Zn-PEAA is:

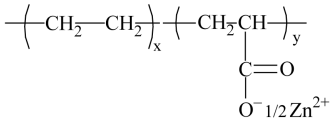

Scheme 1

Sample preparation

Melt processing of Zn PEAA was carried out in a Brabender Plasticorder at 180°C for 3 min at a rotor speed of 60 rpm. After melt mixing, the sample was taken out and compression molded between mylar sheets in an electrically heated press at 150°C, for 3 min, and finally cooled under pressure. The sheet was kept at room temperature for more than 24 h prior to any test.

Iso-DSC and MDSC studies

Isothermal DSC was conducted using DSC 2920 from TA Instruments. Helium was used as the purge gas (50 mL min^{-1}) due to its high thermal conductivity and low coefficient of thermal expansion, facilitating fast response and minimizing baseline curvature. Indium (10 mg) was used for cell constant and temperature calibrations using experimental conditions. The sample mass was 5–10 mg. The sample was first heated from 30–120°C at 20°C min^{-1}, then rapidly cooled down to various isothermal temperatures, which are 78, 80, 82, 83, 84, 85 and 87°C respectively, and held at each temperature for 40 min. This is because this temperature is high enough to melt poly(ethylene) crystal, and to destroy the thermal history of sample preparation. The heat flow *vs*. time was measured during isothermal period. Integration across the exothermal area was used to calculate the heat of fusion for various isothermal conditions. The degree of crystallinity was evaluated by plotting the fractional area of the isothermal crystallization curve at any time. The TA Instruments Isothermal Kinetics

software was used to obtain the SB (Šesták Berggren) kinetic parameters, which was compared to the Avrami and the Arrhenius data.

MDSC™ was conducted using DSC 2920 from TA Instruments to analyze the melting/crystallization behavior. Helium was used as the purge gas (50 mL min^{-1}). Indium (10 mg) was used for the cell constant and temperature calibrations, and Sapphire (24 mg) was used for the heat capacity calibration under non-isothermal conditions using the hermetic aluminum pans and experimental conditions. The sample mass was 5–10 mg. The sample was first heated from 30–120 at 20°C min^{-1} in DSC, then cooled from 120–30°C at 0.5, 2, 5°C min^{-1} cooling rates respectively, finally heated again from 30–120 at 2°C heating rate under heat only condition with an amplitude of modulation ±0.2°C and period 40 s in MDSC™. The heat flow associated with the transitions in the materials as a function of time and temperature was measured. Thermal analysis software from TA instruments was used to analyze the results. The endothermic peak areas in J g^{-1} were integrated to measure the enthalpy of fusion of various crystal conformations using the perpendicular drop method.

Theory of iso-DSC and MDSC™

Iso-DSC was used to monitor the kinetics of crystallization through evolution of heat flow with time. The data were analyzed using the Avrami equation:

$$\ln(1-\alpha) = kt^r \tag{1}$$

where α is the crystallinity at time t, r is known as the Avrami constant, and k is the rate constant which contains information on rate of nucleation and linear growth.

However, using the Avrami method one can obtain the morphologies being developed and the nucleation process occurring, but it gives no analysis of the actual crystal growth rate. The half-life of crystallization as shown below allows one to calculate the rate coefficient,

$$k' = \ln(2)/t_{1/2}^n \tag{2}$$

where k' is the rate constant at the half-life of crystallization.

If this rate data is plotted *vs*. reciprocal of crystallization temperature, for instantaneous nucleation, a linear relation will result, whereas for sporadic nucleation a linear relation will be found when plotted *vs*. reciprocal of square of temperature. The other models such as Arrhenius equation and the Šesták–Berggren (SB) equation were also applied to analyze the data in this work.

Arrhenius equation: The crystallization rate ($d\alpha/dt$) as measured by DSC can be represented by:

$$d\alpha/dt = k(T)f(\alpha) \tag{3}$$

where $f(\alpha)$ is the conversion level, and $k(T)$ is the specific rate constant that is a function of temperature (T), and can be calculated by the Arrhenius equation:

$$k = Z\exp(E/RT) \tag{4}$$

where Z is the pre-exponential factor, E is the activation energy of crystallization and R is the universal gas constant. The activation energy (E) and the natural logarithm of Z were obtained from the plot of ln$k$ *vs*. $1/T$ respectively, E is obtained from the slope of this plot, and intercept gives the natural logarithm of Z.

For different forms of $f(\alpha)$, the Šesták–Berggren (SB) equation is introduced due to the multi-stage crystallization process of the polymer:

$$f(\alpha) = \alpha^m (1-\alpha)^n \tag{5}$$

where m and n are reaction order constants. By analyzing multi-run data using the TA Instruments Isothermal Kinetics software, m, n, E and Z can be obtained. The r value can be calculated by using Eq. (6):

$$r = 1/[1+\ln(n)- \ln(m+n)] \tag{6}$$

The value of r depends on the type of nuclei and the dimensionality of their growth, and the crystallizing rate [35]. r has the value of 1, 2 and 3 for needle-shaped crystals, plates and spheres respectively.

In the MDSC™ technique, the temperature is the superimposition of a sine wave on the conventional linearly changing temperature program; thus basic temperature modulation equation for the block temperature can be written as:

$$T = T_0 + \beta t + A_T \sin(\omega t) \tag{7}$$

where T_0 is the initial temperature, β is the linear heating rate, A_T is the amplitude, ω is the modulation angular frequency ($2\pi f$) and t is the time.

The equation, which describes the resultant heat flow at any point in a DSC or MDSC™ experiment, is:

$$dQ/dt = C_p\beta + f(T,t) \tag{8}$$

where dQ/dt is the total heat flow, C_p is the heat capacity, β is the heating rate and $f(T,t)$ is the heat flow from the kinetic process. MDSC™ determines the total, as well as the reversing heat flow ($C_p\beta$) and the non-reversing heat flow [$f(T,t)$] to provide increased understanding of complex transitions in materials. MDSC™ records the modulated temperature, the modulated heat flow in response to temperature function and the phase angle of these two harmonic functions. If the change in the temperature is within the harmonic range (which depends on the parameters of the modulation, the actual temperature, the overall heating rate and the power of the heating/cooling devices) a Fourier analysis of the response of the temperature function will result in two functions: the heat capacity (C_p) which is determined mainly by the amplitude of the responses, and the total heat flow which is the average of the heat flow. The reversing component of the total heat flow is then calculated. The non-reversing component is determined from Eq. (9):

$$H_{\text{non-reversing heat flow}} = H_{\text{total heat flow}} - H_{\text{reversing heat flow}} \tag{9}$$

Wide-angle X-ray diffraction studies

The wide-angle X-ray diffraction (XRD) experiment was performed at a Difftech MMA X-ray Diffractometer using CuK_α radiation, which is an Anode tube with 7107 Å wavelength. The scan was performed from 5–70° with step size 0.02° and speed 0.25° min^{-1}. Difftech Traces V5 Spectrum Processing Software was used to analyze the XRD results.

Small-angle X-ray studies

Small-angle X-ray scattering (SAXS) data was obtained at room temperature using compression-molded films and a Bruker SAXS instrument. The sample-to-dector distance was 62.7 cm. The X-ray source was from CuK_α radiation. The wavelength is 1.54 Å. The scan of 2θ was from 0.15 to 5°.

Hot stage optical microscopy

Samples used for hot stage optical microscopy were microtomed to a thickness of 40 μm. The specimens were placed on a microscope slide and a cover glass was fixed over it with silicone adhesive to ensure that the polymer remained flat. The slide was then placed in a Mettler FP82 hot stage and heated at a heating rate 2°C min^{-1} to 120°C, held for 4 min, then cooled to different temperatures at a heating rate of 2°C min^{-1}, finally cooled to 30°C at 0.5°C min^{-1}, while video observation was made using Nikon Labphoto 2 microscope with polariser at a magnification 200×. The images were also recorded on a video and representative images were captured during cooling using IPLab image analysis program and the temperature was recorded at the time of capture.

Results and discussion

The influence of ionic interaction on the melt-crystallization behaviour of poly(ethylene) part of ionomer

Figure 1 shows the melting and crystallization behavior of ethylene ionomer as observed in MDSC™ and DSC runs on heating and cooling modes. From MDSC™ heating run, it is clear that the total heat flow is similar to that obtained from conventional DSC. However, this can now be resolved to represent the thermodynamic and kinetic components of heat flow. Three distinct transitions are evident in the total cycle. The melting of ionomer occurs at about 95°C corresponding to the melting of lamellar crystalline region of PE. The lower temperature peak (at about 50°C) corresponds to an order-disorder transition associated with ionic cluster melting. The exothermic peak during cooling relates to the crystallization of poly(ethylene). The DSC/MDSC™ results show that there are three phases in Zn-PEAA: the crystalline phase, the amorphous phase and the cluster. This result agrees with the proposed model for ethylene-acrylic acid copolymer salts by Bonotto and Bonner [4]. In this model, the crystalline phase with a certain lamellar thickness and the cluster exists separately, and the polymer chain of ionomer interpenetrates into the crystalline and the amorphous phases.

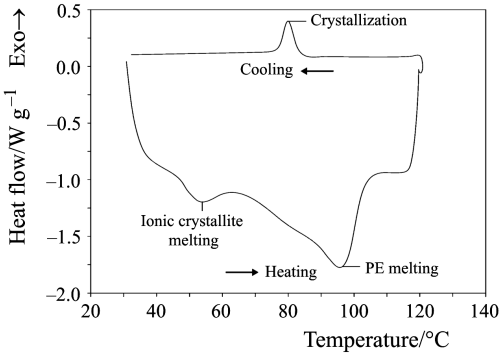

Fig. 1 MDSC and DSC curves showing the melt crystallization behavior of the ionomer

Figure 2 shows the total heat flow *vs*. temperature at three cooling rates, 0.5, 2 and 5°C min^{-1}, for Zn-PEAA and the derivative of modulated temperature *vs*. temperature at 2°C min^{-1}. It shows the heat only conditions for melting with more than 4 modulations during the cycle. From the total heat flow *vs*. temperature, it is obvious that the melting occurs at about 95°C at different cooling rates, and the melting temperature decreases minimally with increasing cooling rate. The curve at 5°C min^{-1} shows only one peak. This indicates that only extended chains exist in the polymer crystal. A shoulder appears on the left-hand side of the main peak at 0.5 and 2°C min^{-1} cooling rates, and the shoulder size increases with decreasing cooling rate. This is ascribed to the presence of folded chains in the polymer crystals. Lower cooling rate for crystallization allows enough time for the molecular chains to align and form a perfectly ordered structure. Even if the polymers were crystallized in a folded chain conformation, it would recrystallize at melting temperature to extended chains. From the plot it is evident that some of the material crystallized as folded chain crystals as non-integral folded chains (NIF). NIFs are generally metastable. At elevated temperature if sufficient time is allowed they can recrystallize to extended chain conformation. The presence of shoulder in some cases can also be due to different morphologies present in the system. However, multiple melt phenomena can also result from one chain conformation. In polymers with narrow molecular mass distri-

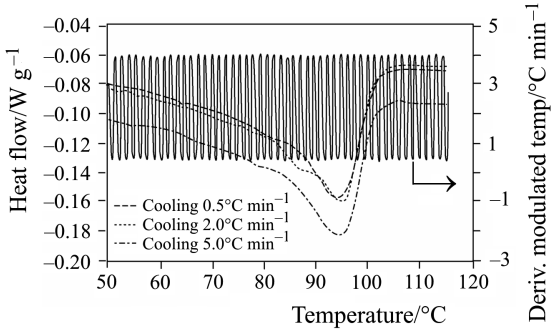

Fig. 2 Plot of the total heat flow *vs*. temperature at three different cooling rates, 0.5, 2 and 5°C min^{-1}

bution (*mmd*), extended chain crystals, which are separated by only repeat unit length can have melting profile at a small difference. It must be mentioned here that different cooling rate only affects the reversing and nonreversing behaviors, and does not change the value of the total heat flow significantly.

Lissajous plot

Examination of the modulated heating rate profile or the Lissajous plot of modulated heat flow *vs*. modulated heating rate also provides an indication that reasonable conditions were used. The Lissajous figures are obtained when plotting the time-dependent heat flow HF(t) of MDSC™ *vs*. the change of the sample temperature $T_s(t)$ or heating rate T. The typical plot gives an elliptical Lissajous plot, as long as the heat capacity is constant over the modulation period and a steady state is maintained. The changes in the ellipse shape and its slope occur normally near a transition. Change in the slope is caused by the change of heat capacity before and during melting. In order to get some information on steady state, Lissajous plot was made before and after the transition. Figure 3 shows the Lissajous plot of Zn-PEAA at 2°C min^{-1} cooling rate. It shows that the change of the slope is very little, or the heat capacity changes little before and after the melting. This indicates after melting a steady state is obtained.

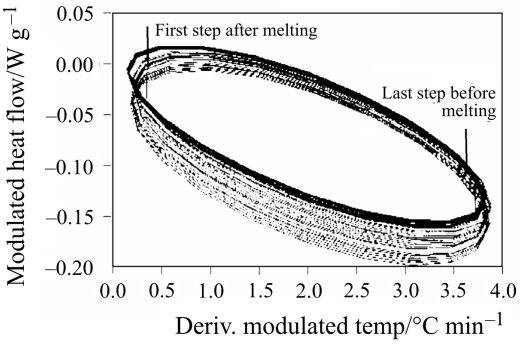

Fig. 3 Lissajous plot of Zn-PEAA at 2°C min^{-1} cooling rate

Figure 4 shows the reversing and non-reversing heat flows *vs*. temperature of the ionomer at a 2°C min^{-1} heating rate. It is obvious that melting of ionomer occurs in the reversing as well as non-reversing heat flow. One peak appears in the reserving heat flow, and the shoulder is present in the non-reversing heat flow. This indicates that melting of extended chains occurs in both the reversing and the non-reversing heat flows, and recrystallization of folded chains to extended conformation occurs only in the non-reversing heat flow. Therefore, the formation of folded chains is time dependent. In this case folded chains were formed at slower cooling rate. The shoulder to the poly(ethylene) melting peak can be clearly seen in the total heat flow component (Fig. 2) and the non-reversing heat flow component (Fig. 4) at low cooling rates. Kovacs and Gonthier [36], and recently Cheng and Chen [37] explained that the shoulder corresponds not only to the different types of folding but can be due to dif-

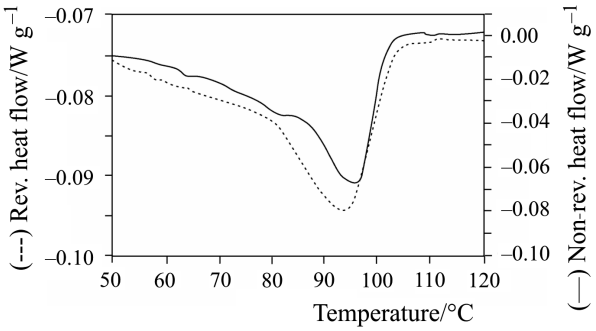

Fig. 4 The reversing and the non-reversing heat flows *vs*. temperature for Zn-PEAA at 2°C min^{-1} heating rate

ferent morphologies present in the system. From Fig. 4, it is obvious that melting temperature is lower in the reversing heat flow than in the non-reversing heat flow indicating the extent of crystal imperfection and recrystallisation.

Table 1 MDSC results of Zn-PEAA

Sample	Cooling rate/ C° min^{-1}	Heat flow/J g^{-1}			Crystallinity/ %	T_c*/ °C
		reversing	non-reversing	total		
Zn-PEAA	0.5	12.1	52.6	64.6	22.3	83.3
	2	15.3	45.4	60.7	20.9	79.1
	5	20.5	40.4	60.8	20.9	76.3

* T_c – crystallization temperature

Table 1 lists the total heat flow and its distribution in the reversing and the non-reversing components, the crystallinity and the crystallization temperature at different cooling rates for Zn-PEAA. A general trend of decreasing enthalpy with increasing cooling rate is evident from Table 1. This indicates that the sample can adopt a more crystalline structure at a lower cooling rate. The fraction of melting in both the signals depends on various experimental parameters [38] such as modulation amplitude, period, underlying heating rate, sample thickness, etc. Under different cooling rates, the contributions of the reversing heat flow and the non-reversing heat flow change, but the total heat flow varies slightly. The non-reversing heat flow decreases with the cooling rate for the ionomer and the reversing component shows the opposite trend (Fig. 5). A critical point is observed on the plot at the 2ºC min^{-1} cooling rate beyond which a marching value is observed in the reversing component. This corresponds to the stability limit of one type of crystal's morphology.

In poly(ethylene), the reversible part of crystallization is controlled by the level of branching. Cser *et al*. [39] reported that the kinetic component of heat flow increases with increasing regularity of their studied poly(ethylene). This could be related to the entanglement density of the melt and the interfacial energy at the

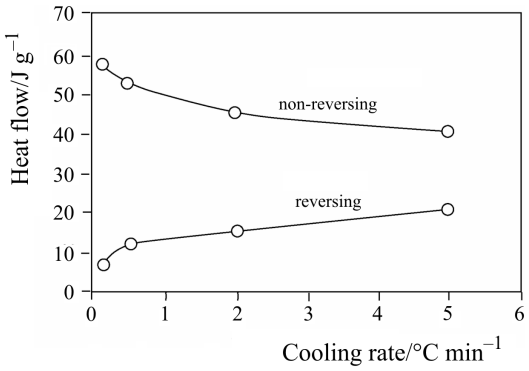

Fig. 5 The non-reversing and the reversing heat flows of the ionomer with the cooling rate

melt-crystal interface. In the linear polymer, melt entanglement density increases because of its favourable structure. However, in branched polymer, that does not occur as branching acts as anchoring points preventing coiling and melting is almost 100% reversible. In ionomers, it is expected that there is a competition between crystallization and clustering that occurs during cooling. In order to form cluster, the ionic or electrostatic interaction between ion pairs in melt has to be higher than the viscoelastic force of the polymer melt. On faster cooling, the ions, which are now solvated in the molten matrix due to their long distance of separation, remain so in the crystal conformation. The change in proportion of two signals during melting thus indicates that a progressive structural variation in the poly(ethylene) part of ionomer occurs resulting in more structural irregularity. Thus, the time dependent part of the heat flow decreases. Recently, Okazaki and Wunderlich [30] proved that the reversibility of polymer melting exists, but only on a molecular or submolecular scale. The reversibility is not lost until the crystal is completely melted. This is because a molecular nucleation is indispensable for the beginning of crystallization of a molecule, or part of a molecule on the surface of a crystal. They concluded that increase in locally reversible melting during melting of polymers is due to the poorer crystals on cold crystallization.

Stability and reversibility of the crystal and the cluster

In order to establish the stability of the crystal structure of the sample, melting runs were repeated five times under the same cooling and heating rates with a modulation of ±0.2°C min^{-1}, period 40 s using MDSC™. Figure 6 shows the thermograms of the multiple runs with the non-reversing heat flow *vs*. temperature. During first heating run, two endothermic peaks are noticed. At the second heating run after cooling, only the high temperature peak is noticed with same melting temperature and same heat of fusion. It must be pointed out here that in the first heating run, the appearance of ionic crystal melting was noticed in the non-reversing component of the heat flow. The results of the total heat flow, the reversing heat flow show little change during the multiple runs. These ionic crystals cannot form immediately after melting. They form by

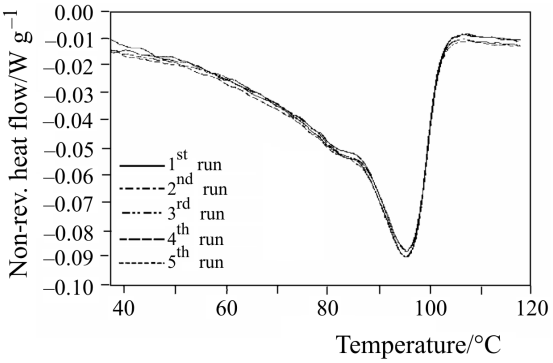

Fig. 6 MDSC curves showing non-reversing heat flow from the multiple runs

a time dependent process after certain period. This also suggests that a molecular motion of the polymer chain in the cluster occurs although the cluster is thought as a physical crosslink. Table 2 lists the MDSC™ results for 1 year aged Zn-PEAA. The same analysis methods were used to get the thermal behavior results. Table 2 shows that the total heat flow decreases slightly with increasing cooling rate. This result indicates that the crystalline structure of the sample is a cooling rate dependent process.

Table 2 MDSC results of Zn-PEAA after one year

Sample	Cooling rate/°C min^{-1}	Total heat flow/J g^{-1}	Crystallinity/%	T_c/°C
Zn-PEAA	0.5	64.0	22.1	83.3
	2.0	61.7	21.3	79.2
	5.0	58.9	20.3	76.3

* T_c – crystallization temperature

Figure 7 shows the DSC curves of a freshly made and 1 year aged samples at 20°C min^{-1} heating rate. The dash line represents the freshly made sample, and the solid line represents the 1 year aged sample. This figure shows that the poly(ethylene) melting temperature does not change with aging, it has high stability. The shoulder does not appear, because the heating rate is too high, and the DSC accuracy is too low to read weak signals. It is interesting to note that both these figures show a first order transition at around 50°C, and on storage at room temperature after 1 year a shift occurs to a higher temperature. The first order transition is related to the ionic cluster transition. The high transition temperature shows that a more perfectly ordered structure is formed. This indicates that forming ionic clusters is a time dependent process. This is because the ionic crystallites are not formation of during cooling from the melt but they gradually develop on aging by a relaxation mechanism. It requires some time to form the ionic crystal structure. By comparing Figs 2 and 7, it is clear that the first order transition does not appear in the second DSC/MDSC™ run. This indicates that the ionic clusters are not formed immediately after melt crystallisation but only

after a prolonged time dependent process. Thus during the melt crystallization study at different cooling rates, they primarily remain in a disordered state. They remain dispersed in the hydrophobic polymer matrix or exist in the amorphous phase or the crystalline surface, hence increase the structural irregularity and clusters cannot form. Over time clustering of the polar group can occur due to the rejection of the polar groups from the hydrophobic matrix.

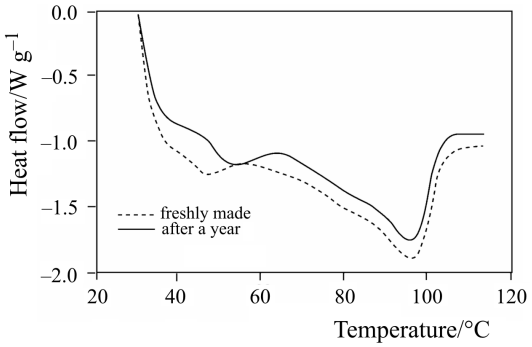

Fig. 7 DSC curves of a freshly made and 1 year aged samples at 20°C min^{-1} heating rate

Generally, there is no doubt that the higher temperature peak is attributed to PE melting. However, the assignment of the lower temperature peak is still a controversial topic. Marx and Cooper [40] first mentioned the lower temperature peak. They observed this peak only after extended storage (1 week to 1 month) of poly(ethylene) methacrylic acid at room temperature. They attributed this phenomenon to the melting of crystallities consisting of short imperfect poly(ethylene) chains. Goddard *et al.* [41] proved this opinion. However, later work by other researchers [42–44] showed that the lower temperature peak corresponded to the order-disorder transition of a first order in ionic clusters. These studies on different ionomers indicated the existence of an order-disorder transition inside the ionic clusters (melting of ionic crystallites) below the poly(ethylene) melting point. Above the lower melting temperature, the ionic clusters are in a disordered state. Hirasawa *et al*. [44] produced a model for order-disorder transition of ionic clusters. Kutsumizu *et al*. [21] not only proved the cluster melting corresponding to the lower temperature peak by IR spectral studies, but also pointed out that this transition included two relaxation processes: a faster process (reversible) and a slower process (non-reversible). The slower process means that the ionic crystallites are not formed at the cluster melting temperature during cooling from melt, but develop gradually during aging at room temperature. Similar observation is made from our DSC results. It is important to remember that the cross-linking in ionomers is not permanent. Tsujita *et al*. [19] have reported that the lamella thickening of ethylene ionomer shows similar behavior to PE even with the existence of clusters. This indicates an incorporation of mobile ethylene unit into the lamella crystal and the existence of mobile chain in cluster. The mobile polymer chain affects the formation of cluster from the melting state above the melting temperature. So the formation of clusters takes a longer time. Figure 7 also shows that the

transition temperature shifts to the higher temperature due to more ordering and strong ionic interactions resulted during ageing.

Tables 1 and 2 show the crystallinity of Zn-PEAA at different cooling rates for both a freshly made and 1 year-aged sample respectively. The two tables show that the crystallinity and the crystallization temperature increase with decreasing cooling rate. The crystallinity was calculated by ratioing the observed enthalpy to the literature enthalpy. The literature enthalpy for 100% crystalline poly(ethylene) is 290 J g^{-1}. Therefore the crystallinity at different cooling rates can be obtained respectively. The tables show that the crystallinity does not change significantly at this cooling rate range, and is slightly higher at the 0.5°C min^{-1} cooling rate than at the other cooling rates. The crystallization temperature decreased with increasing cooling rate. The lower cooling rate allows the crystallization to start earlier and takes longer time so that perfect crystals can be formed. However, it is noticed that the crystallinities between the freshly made sample and 1 year-aged sample are nearly the same. This indicates that the crystallinity does not change with ageing, and it forms at a comparatively early stage of ageing. The melting temperature does not change. This also confirms the high stability of the PE crystal with physical ageing. Thus the only event that disturbs PE crystallinity is clustering. Similar observation was made by Kohzaki *et al*. [17] for poly(ethylene) methacrylic acid ionomers. Most of the PE ionomers studied have crystallinity in the range of 30% [45]. It must be mentioned here that different test methods can give different crystallinity values. The crystallinity of Zn-PEAA in our work is about 22% and it shows similar crystallization behavior to other poly(ethylene) ionomers.

XRD was used to analyse the poly(ethylene) structure and the crystallinity of the ionomer. Figure 8 shows the plot of counts *vs*. scattering angle (2θ). It consists of a sharp peak with two satellite peaks. The sharp peak at 20.47° (2θ) corresponds to the poly(ethylene) crystal. The other two satellite peaks represent the amorphous phase. The space between the two layers of the crystals (*d*) can be calculated using the equation: $d=\lambda/\sin 2\theta$ (where λ=1.54 Å, 2θ=20.47º). So *d* spacing is 4.40 Å. The peak can be curve fitted to three relevant peaks respectively. From the resolved peaks, the ionomer structure and the crystallinity information can be obtained, such as the crossing angle for each phase, the peak area value, etc. By adding each of the peak areas together, the total area value can be

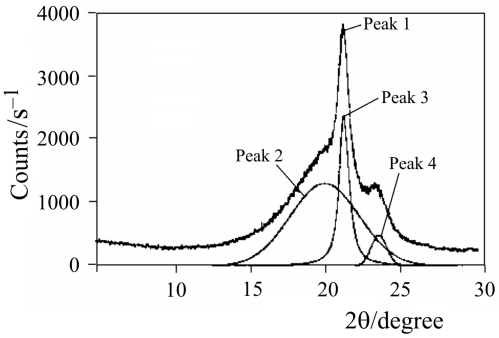

Fig. 8 XRD patterns of the ionomer

obtained. The ratio of each area/total area shows the corresponding phase component in the ionomer. Table 3 lists Zn-PEAA XRD results. From Table 3, the crystallinity of Zn-PEAA is 24%. This value is close to the value obtained from the MDSC™ results. The values between these two results vary slightly due to different test methods.

Table 3 Zn-PEAA XRD results

Peak name	Angle area range/°	Peak total area/counts	Proportion in Zn-PEAA/%
Peak 1 (Amorphous phase)	13.98–26.00	361210	70
Peak 2 (Crystal phase)	18.56–24.20	124330	24
Peak 3 (Amorphous phase)	22.14–24.94	30417	6

The kinetics of the crystallization process and the type of Zn-PEAA using iso-DSC

Development of crystallinity with time at a constant temperature is shown in the crystallization isotherms of Fig. 9. The sigmoidal shape of the isotherm indicates that crystallization of ionomer follows a general nucleation and growth processes. It is obvious that the crystallinity increases with increasing time at each temperature, and the rate of crystallization (slope) decreases with increasing the temperature. The crystallization finished in less than 2 min at 78°C while it takes nearly 20 min at 87°C. This indicates that crystallizing and melting exist at the same time when the isothermal temperature is close to the melting temperature. From this figure, the time for 50% crystallization ($t_{1/2}$) can be obtained at each temperature. k_i is calculated at each temperature using Eq. (2). In Table 4, the values of r, k, k_i and $t_{1/2}$ are listed respectively at each temperature. The crystallization rate strongly depends on temperature. As T_c decreases, the rate increases. Figure 10 shows the Avrami plot of logarithmic rate *vs*. ln(t). It shows the same feature as Fig. 8. From the figure it is clear that the Avrami equation fits well for ionomer at the experimental isothermal conditions. The value of Avrami exponent (the slope) lies between 2.21–2.51 (except for temperatures 82 and 87°C).

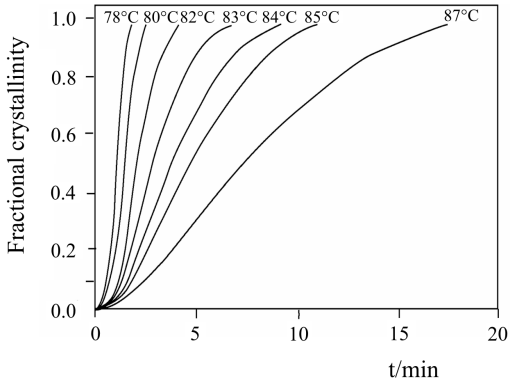

Fig. 9 Fractional crystallinity *vs*. time at various temperatures

Table 4 Ionomer Iso-DSC results using different methods

Autocal. data					Avrami		
Iso-temperature/°C	T_c*/°C	k	r	n	k	$t_{1/2}$	k_i
78	77.9	3.29	2.62	2.21	0.61	0.97	0.74
80	79.8	1.42	2.71	2.29	0.31	1.36	0.34
82	81.7	1.06	1.67	2.95	0.08	2.06	0.08
83	82.7	0.614	1.56	2.51	0.05	2.77	0.05
84	83.7	0.4	1.51	2.47	0.03	3.68	0.03
85	84.7	0.24	1.41	2.27	0.02	4.62	0.02
87	86.7	0.083	1.32	1.86	0.02	7.33	0.02

* T_c – crystallization temperature

Arrhenius equation is also utilized to calculate the values of k, Z and E using Eq. (4) and Fig. 9. The results from Avrami model are listed in Table 4. An exponent of 2 is related to heterogeneous nucleation and it begins with a fixed number of nuclei after which no further growth occurs.

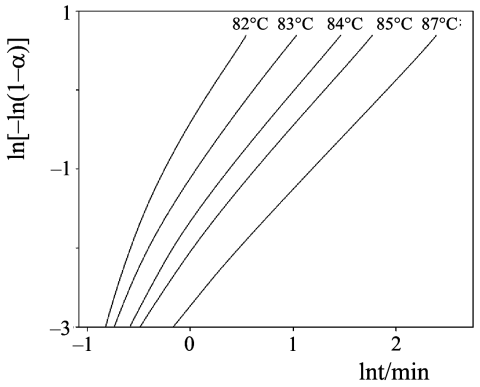

Fig. 10 Avrami plot *vs*. ln*t* of the ionomer

SB equation is also applied to study crystallinity with rate. Figure 11 shows the log of reaction rate *vs*. lg conversion term using the SB equation at 82°C. All individual points fall close to the line indicating the applicability of the SB method for ionomer. From this figure, the values of n, m and k at 82ºC can be obtained. Figure 12 presents conversion time *vs*. temperature for a family of curves ranging from 1 to 90% conversion. Conversion time increases with increasing temperature at each conversion. Low conversion takes short time. The crystallization takes longer time at high temperature than at lower temperature. Also we can estimate the sample behavior from Fig. 12 under conditions not tested. The values of k, k_i, n are listed in Table 4. Similar to the Avrami exponent, the value of r depends on the nature of nuclei, their growth rate etc.

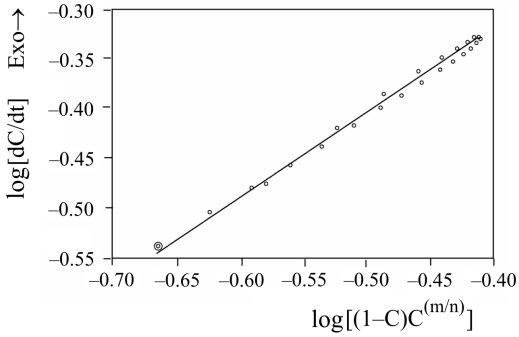

Fig. 11 Plot of log of reaction rate *vs*. the SB log conversion term

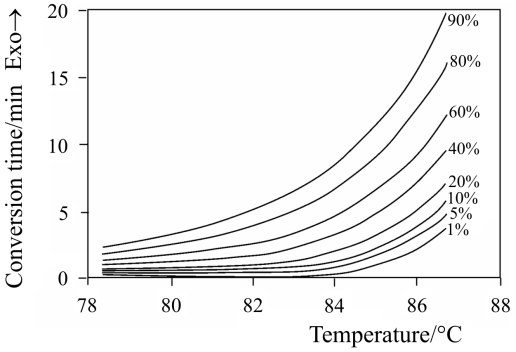

Fig. 12 Plot of the conversion time *vs*. temperature from 1 to 90% conversion

Table 4 shows that k and k_i decrease with increasing temperature, and $t_{1/2}$ increases. The rate of crystallization is slower at higher temperature because crystallization occurs with partial melting when the temperature is close to the melting temperature. The value of the time exponent (Avrami exponent), which is a result of the combination of nucleation type and growth morphology is summarized in the same Table. For systems which are opaque or in which the morphological features are too small to visualize in optical microscope, this still remains a valuable and simple approach for morphological estimation. With different models, the values of k are different, but the agreement between k and k_i in the Avrami model is quite good. This shows that the Avrami model is suitable for Zn-PEAA. However, decreasing the crystallization temperature does not show a regular decrease in r value. Such a low range of r value indicates in its limit an instantaneous type of crystal growth with a fixed number of nuclei. The nuclei grow at early stage with no additional nuclei forming at a later stage. A simple approach to verify the relative growth rate is to use the concept of half-time. The basic growth curves shown in Fig. 9 can be used to rate study by taking the reciprocal of the time taken for the process to half complete. When these data are plotted *vs*. reciprocal of supercooling (Fig. 13), a linear relation was found which indicates instantaneous nature of nucleation. Additionally, the morphology of crystals approximates a needle-shaped crystals and/or plates. At higher temperature, the crystals are more needle-shaped, the plate like structure appears at lower

temperatures. This means that the crystal structure is temperature dependent. Thus the crystalline morphology of poly(ethylene) part of the ionomer does not correspond to a spherulitic material [45] like PE but to a nonspherulitic (lamellar) structure as seen from the iso-DSC results. It is possible that ionization reduces the ease of spherulitic formation of poly(ethylene) part, which results from breakdown of folded chain lamellae originating from the core of spherulite and are more like fringed micelles. The melt interfacial tension is thus believed to be different from pure PE due to the presence of polar cluster.

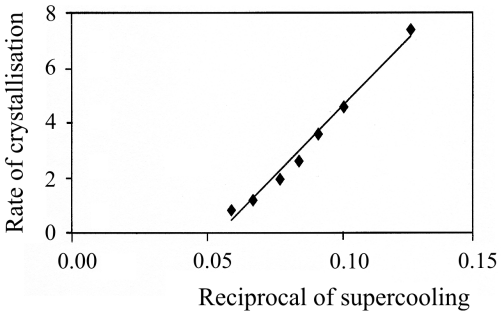

Fig. 13 Rate of crystallization *vs*. reciprocal of supercooling

However, the morphology of the poly(ethylene) part of the ionized copolymer is not so far well understood. Hot stage microstage was done to understand the morphology of ionized sample. The values of *r* for both the SB model and Avrami model are similar. The values of the activation energy using the SB model (265 kJ mol^{-1}) and Arrhenius model (202.7 kJ mol^{-1}) show some variations, however, the values of *Z* are widely different.

Hot stage polarized optical microscopy

Figure 14 shows micrographs of pure poly(ethylene) ionomer after crystallization for various times (from 0–120 min) after cooling from the melt. Polarized optical microscope pictures of the pure poly(ethylene) ionomer is shown in Fig. 14a at 100°C in the melt form, Fig. 14b at 87.5°C shows appearance or onset of crystals, Fig. 14c at 85.0°C displays more crystals, and at 58.0°C (Fig. 14d) even spread of small fine crystals is clearly noticed.

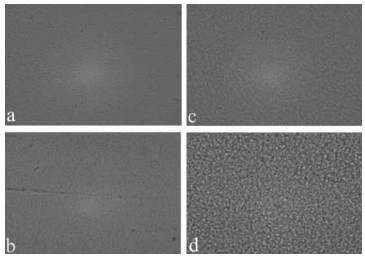

Fig. 14 Polarized optical microscope pictures of the pure poly(ethylene) ionomer, a – 100°C initial, melted form; b – 87.5°C slight crystals; c – 85.0°C more crystals; d – 58.0°C spread of small fine crystals

The onset of crystallization was detected from the initial appearance of the nuclei at a cooling rate of 2°C min^{-1} following melting at 100°C. The figure shows the images of PE crystal. It is observed that fine crystals occupy the complete area after 120 min and amorphous regions exist in the interspherulitic area. However, less defined crystals of ionomer due to ionic group is evident under HSOM. It indicates a lower level of crystallinity as observed from MDSC™, and WAXS.

Studies on the cluster behaviors and the morphology of the cluster

SAXS was used to get the information about ionic domains. Figure 15 shows the curve of the scattered intensity as a function of the scattering angle (2θ, degrees) for Zn-PEAA. The scattering angle range was from 0.15 to 5°. The figure shows a single narrow peak at around 2θ=0.69°, and an upturn in intensity at a low enough angle. The single narrow peak is due to ionic association. It is caused by the aggregation of the ionic groups of $–COOZn_{1/2}$ in the ionomer. The appearance of this peak in the SAXS pattern thus proves the existence of ion aggregation in the ionomer. The equation $d=\lambda/\sin(2\theta)$ was used to calculate the cluster domain diameter, where d is the cluster domain diameter (Bragg spacing), λ is the X-ray wavelength (the CuK_α value is 1.54 Å), 2θ is the scattering angle (2θ=0.69°). So the d value is 127.88 Å. This characteristic peak has been observed in many other ionomers [3, 6, 12]. According to the cluster model proposed by Eisenberg [5], several ion aggregations form multiplets. As the ion content is increased, the multiplets come closer and their distances decrease, and some poly(ethylene) chains get entrapped between the multiplets. When this region is large enough, it forms a cluster, with its own characteristic, and shows microphase separated behavior. A number of multiplets thus form a cluster domain. This domain is found to be greater than 50–100 Å in dimensions. Some models suggested that the salt groups aggregate large enough to form ionic clusters, the cluster size is about 100 Å in diameter. Wilson *et al*. [46] explained from the SAXS result that a peak corresponded to a Bragg spacing of about 20 Å appears in the X-ray scattering from ionomers. Five repeat units are thus minimum to form ionic phase domains. The calculated cluster domain in our study is 127.88 Å. The ion contents exist in the ionomer not only as multiplets, but also that the clusters are formed by the aggregation of the multiplets. The Zn-PEAA peak shifts to the lower scattering vector compared to that of Na-PMAA (polymethyl acrylic acid neutralised with

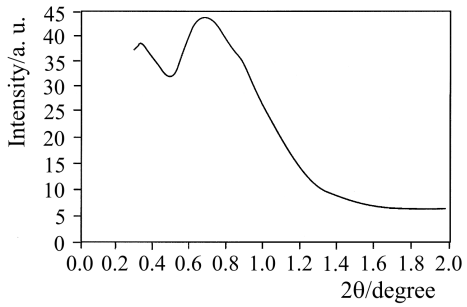

Fig. 15 Plot of the scattered intensity as a function of the scattering angle (SAXS)

sodium salts) because of larger cation size. Galambos *et al*. [47] studied sulfonated atactic polystyrene by DSC, and observed a distinct transition at 180°C corresponding to the development of ion-rich microdomains or clusters. However, the upturn disappears when water or polar solvents exist in the clusters.

Conclusions

Introducing ionic groups into polymer affects the crystallization behavior of poly(ethylene) part of ionomer. The study of iso-DSC reveals that the crystal type of the poly(ethylene) chains in the ionomer is platelike and needle-shaped depending on the temperature, which is different from the crystals of poly(ethylene). The MDSC™ results provide very useful information on melt-crystallization behaviour of ionomer. Melting of ionomer occurs in reversing as well as non-reversing heat flow. Changing cooling rate only changes the contribution of the reversing and the non-reversing components. X-ray studies show that the ionic aggregation and crystalline structure exist in Zn-PEAA. The results of MDSC and XRD show that the polymer structure includes crystals and amorphous regions, and the crystallinity is about 22% (MDSC™). The size of the cluster domain calculated from the SAXS results is 127 Å. The MDSC™ results indicate that the formation of the clusters is a time-dependent process. The melting of ionic crystallites is kinetic in nature and the crystallites developed by a relaxation mechanism. The existence of the ionic aggregation seems to influence the interfacial interaction of the melt and the crystal structure of the ionomer.

References

1 L. Holiday, Ionic Polymer, London, Applied Science Publishers, 1975.
2 A. Eisenberg and J.-S. Kim, Introduction to Ionomers, Wiley, New York 1998.
3 R. Longworth and D. J. Vaughan, Nature, 218 (1968) 85.
4 S. Bonotto and E. F. Bonner, Macromolecules, 1 (1968) 510.
5 A. Eisenberg, Macromolecules, 3 (1970) 147.
6 C. L. Marx, D. F. Caulfield and S. L. Cooper, Macromolecules, 6 (1973) 344.
7 W. J. MacKnight, W. P. Taggart and R. S. Stein, J. Polymer Sci., Symposium, 45 (1974) 113.
8 M. Pineri, C. Meyer, A. M. Levelut and M. Lumbert, J. Polym. Sci., Polym. Phys. Ed., 12 (1974) 115.
9 T. R. Earnest, Jr., J. S. Higgins, D. L. Handlin and W. J. MacKnight, Macromolecules, 14 (1981) 192.
10 M. Fujimura, T. Hashimoto and H. Kawai, Macromolecules, 15 (1982) 136.
11 W. C. Forsman, Macromolecules, 15 (1982) 1032.
12 D. J. Yarusso and S. L. Cooper, Macromolecules, 16 (1983) 1871.
13 B. Dreyfus, Macromolecules, 18 (1985) 284.
14 M. Pineri and A. Eisenberg, Eds, Structure and Properties of Ionomers, NATO ASI Series, D. Reidel, Dordrecht 1987.
15 A. Eisenberg, B. Hird and R. B. Moore, Macromolecules, 23 (1990) 4098.

16 Y. Tsujita, K. Shibayama, A. Takizawa and T. Kinoshita, J. Appl. Polymer Sci., 33 (1987) 1307.
17 M. Kohzaki, Y. Tsujita, A. Takizawa and T. Kinoshita, J. Appl. Polymer Sci., 33 (1987) 2393.
18 J.-S. Kim, H. Nah, S.-S. Jarng, W. Kim, Y. Lee and Y.-W. Kim, Polymer, 41 (2000) 3099.
19 Y. Tsujita, S. L. Hsu and W. J. MacKnight, Macromolecules, 14 (1981) 1824.
20 H. Tachino, H. Hara, E. Hirasawa, S. Kutsumizu, K. Tadano and S. Yano, Macromolecules, 26 (1993) 752.
21 S. Kutsumizu, Macromolecules, 32 (1999) 6340.
22 M. Avrami, J. Chem. Phys., 7 (1939) 1103.
23 J. Šesták and G. Berggren, Thermochim. Acta, 3 (1971) 1.
24 J. N. Hay, P. A. Fitzgerald and M. Wiles, Polymer, 17 (1976) 1015.
25 J. A. Haigh, C. Nguyen, R. G. Alamo and L. Mandlekern, J. Therm. Anal. Cal., 59 (2000) 435.
26 K. Nagarajan, K. Levon and A. S. Myerson, J. Therm. Anal. Cal., 59 (2000) 497.
27 E. Hirasawa, Y. Yamamoto, K. Tadano and S. Yano, J. Appl. Polym. Sci., 42 (1991) 351.
28 M. Reading, Trends Polym. Sci., 8 (1993) 248.
29 B. Wunderlich, Y. Jin and A. Boller, Thermochim. Acta, 238 (1994) 277.
30 I. Okazaki and B. Wunderlich, Macromolecules, 30 (1997) 1758.
31 S. Bonotto and E. Bonner, Macromolecules, 11 (1968) 510.
32 E. P. Otocka and T. K. Kwei, Polymer Preprints, 9 (1968) 1.
33 E. P. Otocka and T. K. Kwei, SPE Antec, 15 (1969) 23.
34 W. J. MacKnight and F. A. Emerson, Polymer Preprints, 12 (1971) 149.
35 J. Šesták, Thermophysical Properties of Solids, Their Measurements and Theoretical Analysis, Elsevier, Amsterdam 1984, p. 190.
36 A. J. Kovács, A. Gonthier and C. Straupe, J. Polym. Sci.: Polym. Symp., 50 (1975) 283.
37 S. Z. D. Cheng and J. Chen, J. Polym. Sci.: ptB: Polym. Phys., 29 (1991) 311.
38 E. Verdonck, K. Schaap and L. C. Thomas, Int. J. Pharm., 192 (1999) 3.
39 F. Cser, F. Rasoul and E. Kosior, J. Therm. Anal. Cal., 52 (1998) 293.
40 C. L. Marx and S. L. Cooper, J. Macromol. Sci. Phys., B9 (1974) 19.
41 R. J. Goddard, B. P. Grady and S. L. Cooper, Macromolecules, 27 (1994) 1710.
42 K. Tadano, E. Hirasawa, Y. Yamamoto, H. Yamamoto and S. Yano, Jpn. J. Appl. Phys., 24 (1987) L1440.
43 K. Tadano, E. Hirasawa, H. Yamamoto and S. Yano, Macromolecules, 22 (1989) 226.
44 E. Hirasawa, Y. Yamamoto, K. Tadano and S. Yano, Macromolecules, 22 (1989) 2776.
45 P. J. Phillips, Handbook of Crystal Growth, Elsevier 1994.
46 F. C. Wilson, R. Longworth and D. J. Vaughan, Polym. Prepr. Amer. Chem. Soc. Div. Polym. Chem., 9 (1968) 505.
47 A. F. Galambos, W. B. Stockton, J. T. Koberstein, A. Sen, R. A. Weiss and T. P. Russell, Macromolecules, 20 (1987) 3091.
48 W. J. MacKnight, L. W. McKenma and B. E. Read, J. App. Phys., 38 (1967) 4208.